Understanding the Conformational Dependence of Spin–Spin Coupling Constants: Through-Bond and Through-Space $J(^{31}P,^{31}P)$ Coupling in Tetraphosphane-1,4-diides $[M(L)_x]_2[P_4R_4]$

Martin Kaupp,*[a] Alexander Patrakov,[a] Roman Reviakine,[a] and Olga L. Malkina[b]

Abstract: The characteristic dependence of $J(^{31}P,^{31}P)$ spin–spin coupling constants of alkali metal tetraphosphane-1,4-diides on structure and composition has been analyzed by density functional methods. The computations confirm that the structure of the contact ion pairs is conserved in solution. Calculations on model systems $M_2P_4H_4$, on naked $P_4H_4^{2-}$ anions, and on models including point charges, show that the role of the cations is mainly structural and to a smaller extent electrostatic. Three of the four $J(P,P)$ coupling constants depend characteristically on the conformation of the anion, which in turn is determined by the substituents R and by cation–anion interactions. Several couplings exhibit a large through-space component and are thus strongly dependent on the relative orientation of nonbonding electron pairs on the phosphorus atoms involved. This is shown by visualization of coupling pathways using the recently introduced coupling energy density (CED), in combination with the electron localization function (ELF).

Keywords: coupling energy density · electron localization function · NMR spectroscopy · spin–spin coupling · through-space coupling

Introduction

The pathways of nuclear spin–spin coupling are of substantial interest for the interpretation of NMR spectra.[1] Topics of current discussion include "through-space" versus "through-bond" couplings,[1–3] couplings across hydrogen bonds in proteins (this touches the question of covalency of hydrogen bonds),[4–6] or coupling pathways in multicyclic organic or organometallic compounds (e.g. questions of "through-metal" or "through-backbone" coupling in chelate complexes[1,2,7]). In the case of contact ion pairs in solution, the question frequently arises to what extent a metal cation is involved in the coupling between different nuclei of the counteranion, and to which extent "through-space" and "through-bond" couplings dominate.[8] In the case of polyphosphanes,[9] polyphosphanides,[10] or polyphosphenides,[11] an influence of the relative orientation of phosphorus lone pairs on two- or three-bond couplings has long been assumed but was not substantiated theoretically. It is these types of questions that we address in this work, using quantum chemical calculations of spin–spin coupling constants, together with a recently developed approach of visualizing coupling pathways by real-space functions.

We will concentrate our analyses on a series of four alkali metal tetraphosphane-1,4-diides, which were recently studied by Wolf et al.,[12] including improved syntheses, crystal structure analyses, and solution NMR spectra. Interestingly, the crystal structures indicated two different types of coordination of the alkali metal cations to the anions: $[K(thf)_3]_2[P_4Mes_4]$ and $[Na(thf)_2]_2[P_4Mes_4]$ exhibit a coordination of the cations by all four phosphorus atoms in a bicyclic arrangement, dominated by the formation of four-membered chelate rings of the alkali metal with the $(P_4R_4)^{2-}$ ligand (type I in Figure 1).[12] In contrast, $[Na(thf)_{2,5}]_2[P_4Ph_4]$ and $[Na(thf)_2]_2[P_4tBu_4]$ crystallize in a structurally distinct form (type II in Figure 1), with coordination only to the terminal phosphorus atoms of the tetraphosphane-1,4-diide anion. The most characteristic structural feature of this arrangement, which was already proposed by Baudler and co-workers for these species in solution,[13] is the formation of five-membered chelate rings between the tetraphosphanediide ligand and the alkali metal cations. The structures of $[Na_2(thf)_4(tmu)]_2[P_4Ph_4]$, $[Na_2(tmeda)]_2[P_4Ph_4]$, and $[Na_2(dme)]_3$-

[a] Prof. Dr. M. Kaupp, A. Patrakov, Dr. R. Reviakine
Institut für Anorganische Chemie, Universität Würzburg
Am Hubland, 97074 Würzburg (Germany)
Fax: (+49) 931-888-7135
E-mail: kaupp@mail.uni-wuerzburg.de

[b] Dr. O. L. Malkina
Institute of Inorganic Chemistry
Slovak Academy of Sciences
Dubravska Cesta 9, 84536 Bratislava (Slovakia)

 DOI: 10.1002/chem.200401111

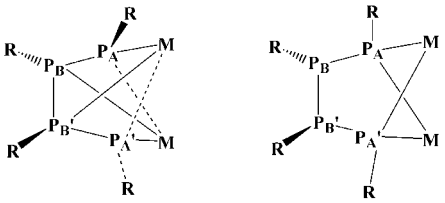

Figure 1. Connectivity and structure of the two types of alkali metal tetraphosphane-1,4-diides.[12] Type I, found for $[Na(thf)_2]_2[P_4Mes_4]$ and $[K(thf)_3]_2[P_4Mes_4]$. Type II, found for $[Na(thf)_{2.5}]_2[P_4Ph_4]$ and $[Na(thf)_2]_2[P_4tBu_4]$.

$[P_4Ph_4]$ found by another group[14] are very similar to that found for $[Na(thf)_{2.5}]_2[P_4Ph_4]$. Most interestingly, the solution ^{31}P NMR spectra of these two classes of compounds exhibited similar chemical shifts but notably different spin–spin coupling constants.[12] The remarkable trends in the coupling constants of these species and comparison of these values with those of related five-membered heterocycles P_4R_4X (X = CH_2 or a heteroatom) suggested that these contact ion pairs are preserved in their solid-state arrangements upon dissolution. The "type I" compounds exhibited relatively small negative $^1J(P_B,P_{B'})$ near −120 Hz, appreciably positive $^2J(P_A,P_{B'})$ of about +107 to 120 Hz, and very small $^3J(P_A,P_{A'})$. In contrast, the "type II" complexes were found to have larger negative $^1J(P_B,P_{B'})$ near −310 Hz, very small negative $^2J(P_A,P_{B'})$, and strongly positive $^3J(P_A,P_{A'})$ near +200 to 310 Hz.[12] The origin of these differences in coupling constants is unclear. In general, coupling pathways are not well understood in many related cases, where alkali or alkaline earth cations bridge different atoms in anionic compounds. There has been speculation about direct involvement of the cations in the coupling pathways.[8,12] Alternatively, the main role of the cation coordination for the spin–spin coupling could be the enforcement of a certain nuclear arrangement in the anion (or between separate anions). We will show here by suitable quantum chemical analyses that the latter explanation is closer to reality. The results may also have bearing on the question of spin–spin coupling constants across hydrogen bonds in proteins, where a structural role of the bridging protons appears more important than any covalent bonding through them.[5,6,15]

Computational Details

To reduce the computational effort of the individual calculations and thus to be able to carry out a systematic study of various effects, we limited our study to truncated model systems. These were designed to incorporate the main structural and electronic features that determine the spin–spin couplings of interest. Starting from the X-ray structures of the four compounds, we removed the coordinating THF solvent molecules from the metal cations and replaced the organic substituents by hydrogen atoms (a standard P–H bond length of 1.43 Å was assumed) to arrive at model complexes $M_2[P_4H_4]$ (M = K, Na). The model structures obtained in this way will be denoted by, e.g., "$Na_2P_4Mes_4$", and so on (cf. Tables 1 and 2).

Initially, all remaining structural parameters were kept at the values taken from the X-ray structure analyses.[12] The role of the cations was studied a) by calculations on the free $P_4H_4^{2-}$ anions, and b) by replacing the cations with unit point charges. Additional calculations on the free anions studied the dependence of the coupling constants on various conformational degrees of freedom, in particular on the dihedral angle α (P_A-P_B-$P_{B'}$-$P_{A'}$). In this case, α was varied in steps of 10°, and the other dihedral angles β (H[P_A]-P_A-P_B-$P_{B'}$) and γ (H[P_B]-P_B-P_A-$P_{B'}$), as well as the H-P-P bond angles were allowed to relax to different conformers (P–P and P–H distances, as well as P-P-P bond angles were kept at average values: P_A–P_B 2.170 Å, P_B–$P_{B'}$ 2.235 Å, P_A-P_B-$P_{B'}$ 105.0°). These partial structure optimizations were carried out with the Gaussian03 program,[16] the B3PW91 functional,[17,18] a pseudopotential and DZP valence basis set on P,[19] and a DZP basis on H.[20] We note that the isolated free anions are not expected to be stable entities in the gas phase or even in solvent-separated ion pair triples.[14] They are nevertheless useful models to understand conformational effects on the coupling constants. Except for the "$Na_2P_4Ph_4$" structure, which arises from a C_2 symmetrical site in the crystal structure of the substituted compound,[12] the experimental structures are only approximately symmetrical. We report nevertheless couplings always just for one of two "almost" equivalent pairs of nuclei, as the slight differences between pairs are insignificant. Note that the experimentally determined structures correspond to the $P_B(R)$/$P_{B'}(R)$ stereoisomers for all systems except for "$Na_2P_4Ph_4$", which represents the *S*,*S* enantiomer.

Calculations of spin–spin coupling constants were performed both with the Gaussian03[16] and ReSpect[21] programs. While we will focus mainly on the Fermi contact (FC) contributions to the couplings, the analytical linear response calculations with Gaussian03 provide also the diamagnetic spin-orbit (DSO), paramagnetic spin-orbit (PSO) and spin-dipolar (SD) contributions to the nonrelativistc couplings (see Table 1). Calculations with ReSpect neglected the SD contribution and used a single finite perturbation theory approach[22] (SFPT) to compute the FC contribution (the PSO and DSO contributions are obtained analytically[22]). The Gaussian03 calculations employed the exchange-correlation functionals BP86[23,24] or B3PW91,[17,18] calculations with Respect used the same functionals and additionally the PP86[24,25] gradient-corrected functional. In all cases we used a DZVP basis[26] on the metal atoms (where present) and Huzinaga–Kutzelnigg IGLO-III basis sets[27] on the P and H atoms.

In the SFPT calculations with ReSpect, the Fermi-contact operator was included in the Hamiltonian as a finite perturbation on the P_A atoms [on P_B for $^1J(P_B,P_{B'})$] with perturbation parameter $\lambda = 0.001$. To avoid numerical errors in the

finite perturbation calculations from inaccurate molecular orbitals, these computations employed EXTRAFINE integration grids with 128 radial shells (corresponding to ca. 22000–24000 points per atom). Calculations in Gaussian03 used the default "finegrid" option, as test calculations with larger grids did not change the results appreciably. Most interpretations of the spin–spin couplings will be based on FC contributions obtained by the SFPT approach with ReSpect.

To visualize coupling pathways, the double finite perturbation theory (DFPT) approach of Malkina and Malkin[28] was used, with finite perturbation parameters $|\lambda_1| = |\lambda_2| = 0.01$ on the two P atoms coupled, and all other computational parameters as described above. The ReSpect implementation[21] was used. From these calculations, we extracted the coupling energy density (CED),[1,28] $\varepsilon_{MN}(r)$. The CED is the difference of two energy densities for DFPT calculations with parallel and antiparallel nuclear spins on the two nuclei N and M, defined such that the space integral of $\varepsilon_{MN}(r)$ provides the reduced coupling constant K_{MN} [Eq. (1)].

$$J_{MN} = \frac{\hbar}{2\pi}\gamma_M\gamma_N \cdot K_{MN} = \frac{1}{2}\int [\varepsilon^{\uparrow\uparrow}(r) - \varepsilon^{\uparrow\downarrow}(r)]\mathrm{d}V = \frac{\hbar}{2\pi}\gamma_M\gamma_N \int \varepsilon_{MN}(r)\mathrm{d}V \quad (1)$$

Here, J_{MN} is the coupling constant, and γ_M/γ_N are the nuclear gyromagnetic ratios of nuclei N and M. The CED is displayed in isosurface plots with the Molekel visualization program.[29] Similarly, isosurface plots of the electron localization function (ELF[30]) are displayed with Molekel (the ELF was calculated using TopMod[31]). Natural atomic charges from natural population analyses (NPA)[32] were obtained with the built-in NBO3.0 routines of Gaussian03.

Results and Discussion

Comparison of methods and models: Table 1 provides both Gaussian03 and ReSpect results for the individual contributions to the coupling constants for the $M_2P_4H_4$ model systems and compares the total computed couplings to the experimental data for the "real systems" in solution. Apart from the missing SD contributions in the ReSpect calculations, results with the different programs and methodologies agree very well with each other. The couplings are almost invariably dominated by the FC term, whereas the DSO term is negligible. The PSO and SD terms are smaller than the FC contribution but contribute nonnegligibly to the short-range couplings $J(P_A,P_B)$ and $J(P_B,P_{B'})$. Notably, the PSO term is of similar magnitude and negative for both of these couplings for the structures with small dihedral angle α (type II, "$Na_2P_4Ph_4$" and "$Na_2P_4tBu_4$"), whereas it is more negative for $J(P_A,P_B)$ but very small and positive for $J(P_B,P_{B'})$ for the remaining two cases with α near 75° (type I, "$Na_2P_4Mes_4$" and "$K_2P_4Mes_4$"; Table 1). The SD term is positive for both couplings (of similar magnitude for both couplings with type II structures, larger for $J(P_A,P_B)$ with type I).

Given the drastic simplifications of the gas-phase models compared with the real systems in solution, agreement of the total computed couplings is remarkably good for both type I systems, where deviations of the overall results (including the SD term from Gaussian03) from experiment are mostly below 35 Hz except for $J(P_B,P_{B'})$ in "$Na_2P_4Mes_4$" which is 60 Hz too positive after inclusion of the (positive) SD contribution. The agreement is still reasonable for the type II systems, but deviations from experiment are +130 Hz for $J(P_A,P_{A'})$ in "$Na_2P_4Ph_4$" and +90 Hz for $J(P_A,P_B)$ in "$Na_2P_4tBu_4$". In these cases, the influence of the counterions appears also to be particularly large (see below), and thus the removal of the solvent sphere from the cation in our models may be a more severe approximation. In any case, however, the calculations reproduce faithfully the major differences in all couplings between the type I and II systems. This holds already when we consider only the FC contributions. We may thus base our following analyses and interpretations on the FC contributions alone. As the SFPT results with ReSpect-MAG agree excellently with the CPKS Gaussian03 data (Table 1), we will use the computationally more expedient SFPT calculations for further analysis.

Table 2 evaluates the influence of the exchange-correlation functional, and of further simplifications of our model systems on the FC contributions to the couplings. Spin–spin coupling constants are known to depend appreciably on the exchange-correlation functional used in DFT calculations.[22] Indeed, the present results depend somewhat on the functional, but the differences are not sufficiently large to affect any of the main trends. In particular, all relevant differences in the most interesting $J(P_A,P_{A'})$, $J(P_A,P_{B'})$ and $J(P_B,P_{B'})$ coupling constants are reproduced by all functionals. We will in the following concentrate on results obtained with the B3PW91 hybrid functional.

Replacement of the metal cations by point charges is an acceptable further approximation that may introduce errors up to 30–40 Hz for the largest couplings but still retains the important trends (Table 2). The complete removal of the counterions is a more drastical approximation and leads to larger deviations. Interestingly, these differences appear to be by far most pronounced for the $J(P_A,P_{A'})$ coupling constants of the type II systems "$Na_2P_4Ph_4$" and "$Na_2P_4tBu_4$", where removal of the cations reduces the couplings by about 200 Hz and by about 100 Hz, respectively. In absolute values, the very small $J(P_A,P_{A'})$ couplings in the type I systems appear to be affected much less by removal of the metal cations (due to the small absolute values, percentage changes are nevertheless large). This may reflect stronger interactions between cations and terminal phosphorus atoms in the anions in the type II systems (cf. Figure 1). To test this assumption, we have computed NPA charges for the different structural arrangements of the $M_2P_4H_4$ models (Table 3): In going from the "$K_2P_4Mes_4$" to "$Na_2P_4Mes_4$" to "$Na_2P_4Ph_4$" to "$Na_2P_4tBu_4$" structures, the charge transfer to the metal cations increases. Most notably, however, delocalization of the negative charge from the terminal P_A atoms (the formal bearers of the negative charge) towards the cen-

Table 1. Comparison of computed J(P,P) spin–spin coupling constants [Hz] for $M_2[P_4H_4]$ molecular models of solid-state $[M(thf)_x]_2[P_4R_4]$[a] with experiment, and break down into different contributions.[b]

Model structure		FC		SD[c]		PSO		DSO		Sum[d]	Exptl[e]
"$K_2P_4Mes_4$"	$^1J(P_A,P_B)$	−275.7	(−275.9)	+18.1	(−)	−63.2	(−63.3)	+0.2	(+0.2)	−320.6	−328.5(2)
	$^1J(P_B,P_{B'})$	−132.3	(−132.2)	+36.0	(−)	+4.8	(+4.8)	+0.2	(+0.3)	−91.3	−127.6(2)
$\alpha=75$[f]	$J(P_A,P_{B'})$	+121.7	(+122.6)	+2.7	(−)	+3.1	(+3.1)	0.0	(0.0)	+127.5	+107.2(1)
	$J(P_A,P_{A'})$	+6.5	(+6.7)	−1.7	(−)	−0.4	(−0.4)	0.0	(0.0)	+4.4	+1.5(2)
"Na_2P_4Mes"	$^1J(P_A,P_B)$	−251.3	(−252.1)	+23.1	(−)	−52.8	(−52.9)	+0.2	(+0.2)	−280.8	−309.8(1)
	$^1J(P_B,P_{B'})$	−101.3	(−101.4)	+38.2	(−)	+4.1	(+4.1)	+0.2	(+0.2)	−58.8	−118.3(1)
$\alpha=73$[f]	$J(P_A,P_{B'})$	+127.8	(+126.3)	+1.4	(−)	+0.9	(+0.9)	0.0	(0.0)	+130.1	+120.3(1)
	$J(P_A,P_{A'})$	+8.6	(+8.8)	−3.0	(−)	−1.2	(−1.2)	0.0	(0.0)	+4.4	+3.3(1)
"$Na_2P_4Ph_4$"	$^1J(P_A,P_B)$	−311.1	(−311.8)	+28.3	(−)	−21.5	(−21.5)	+0.2	(+0.2)	−304.1	−323.1(6)
	$^1J(P_B,P_{B'})$	−338.3	(−339.0)	+30.5	(−)	−15.8	(−15.8)	+0.2	(+0.2)	−323.4	−310.2(6)
$\alpha=32$[f]	$J(P_A,P_{B'})$	−15.3	(−15.2)	−1.8	(−)	−3.6	(−3.7)	0.0	(0.0)	−20.7	−12.3(6)
	$J(P_A,P_{A'})$	+409.2	(+409.9)	+9.3	(−)	+13.5	(+13.5)	+0.1	(+0.1)	+432.1	+310.6(7)
"Na_2P_4tBu"	$^1J(P_A,P_B)$	−249.2	(−250.0)	+25.3	(−)	−29.7	(−29.7)	+0.2	(+0.2)	−253.4	−341.1(2)
	$^1J(P_B,P_{B'})$	−316.9	(−317.9)	+27.2	(−)	−10.6	(−10.6)	+0.2	(+0.2)	−300.1	−305.5(2)
$\alpha=9$[f]	$J(P_A,P_{B'})$	−8.5	(−8.8)	−0.4	(−)	−2.3	(−2.3)	0.0	(0.0)	−11.2	−12.6(1)
	$J(P_A,P_{A'})$	+233.8	(+236.0)	+5.8	(−)	+6.6	(+6.6)	+0.1	(+0.1)	+246.3	+200.9(2)

[a] "$K_2P_4Mes_4$" refers to a $K_2P_4H_4$ model, which was constructed from the corresponding structure parameters of $[K(thf)_3]_2[P_4Mes_4]$. Similarly, "Na_2P_4Mes" is $Na_2P_4H_4$ constructed from $[Na(thf)_2]_2[P_4Mes_4]$, "$Na_2P_4Ph_4$" is $Na_2P_4H_4$ corresponding to $[Na(thf)_{2.5}]_2[P_4Ph_4]$, and "$Na_2P_4tBu$" is $Na_2P_4H_4$ constructed from $[Na(thf)_2]_2[P_4tBu_4]$. Structure parameters adapted from ref. [12]. [b] Gaussian03 results at B3PW91/IGLO-III level with corresponding ReSpect-MAG results in parentheses. [c] SD term not available with MAG-ReSpect. [d] Sum of all contributions, provided only for the Gaussian03 CPKS results. [e] Ref. [12]. [f] Dihedral angle α (P_A-P_B-$P_{B'}$-$P_{A'}$) in degrees.

Table 2. Dependence of the Fermi-contact contribution to spin–spin coupling constants [Hz] on exchange-correlation functional and molecular model.[a]

Functional: model: structure[a]	coupling	BP86 complex[b]	PP86 complex[b]	complex[b]	B3PW91 free anion[c]	+point charges[d]	exptl[e]
"$K_2P_4Mes_4$"	$^1J(P_A,P_B)$	−294.2	−319.6	−275.9	−291.8	−251.4	−328.5(2)
	$^1J(P_B,P_{B'})$	−152.9	−170.1	−132.2	−97.6	−100.2	−127.6(2)
$\alpha=75$[b]	$J(P_A,P_{B'})$	+121.1	+123.2	+122.6	+171.6	+114.7	+107.2(1)
	$J(P_A,P_{A'})$	+5.7	+5.2	+6.7	+3.4	+4.0	+1.5(2)
"Na_2P_4Mes"	$^1J(P_A,P_B)$	−269.1	−292.1	−252.1	−298.1	−220.2	−309.8(1)
	$^1J(P_B,P_{B'})$	−114.4	−131.4	−101.4	−78.1	−71.8	−118.3(1)
$\alpha=73$[b]	$J(P_A,P_{B'})$	+128.0	+136.1	+126.3	+181.7	+119.3	+120.3(1)
	$J(P_A,P_{A'})$	+5.7	+3.6	+8.8	+6.1	+5.6	+3.3(1)
"$Na_2P_4Ph_4$"	$^1J(P_A,P_B)$	−338.5	−361.9	−311.8	−344.3	−309.1	−323.1(6)
	$^1J(P_B,P_{B'})$	−360.0	−376.4	−339.0	−322.0	−339.4	−310.2(6)
$\alpha=32$[b]	$J(P_A,P_{B'})$	−10.3	−11.5	−15.2	−27.9	−20.6	−12.3(6)
	$J(P_A,P_{A'})$	+431.8	+468.3	+409.9	+213.1	+446.8	+310.6(7)
"Na_2P_4tBu"	$^1J(P_A,P_B)$	−270.4	−293.2	−250.0	−322.5	−241.1	−341.1(2)
	$^1J(P_B,P_{B'})$	−344.7	−361.0	−317.9	−263.8	−312.2	−305.5(2)
$\alpha=9$[b]	$J(P_A,P_{B'})$	−4.6	−3.0	−8.8	−0.9	−15.7	−12.6(1)
	$J(P_A,P_{A'})$	+223.4	+219.9	+236.0	+133.5	+254.9	+200.9(2)

[a] See footnote a to Table 1. SFPT results with ReSpect-MAG. [b] $M_2P_4H_4$ models. [c] Metal cations removed completely. [d] Metal cations replaced by positive unit charges. [e] See ref. [12].

tral P_B atoms (and to the associated hydrogen atoms) is much more pronounced in the type I than in the type II systems. This confirms roughly the structure-based "bond topology" indicated in Figure 1,[12] even though the distinction in the drawing may be exaggerated. In any case, interactions between metal cations and P_A atoms are more pronounced for the type II structures, in keeping with the larger influence of the cations on the spin–spin couplings. We conclude at this point that the influence of the cations on the couplings for a given structure may in some cases be nonnegligible, and that the nature of the cation effect is largely electrostatic.

But even the free anions reproduce the main structural dependences to be discussed: The coupling constants reflect in particular the dihedral angle $\alpha = d(P_A\text{-}P_B\text{-}P_{B'}\text{-}P_{A'})$ and are

Table 3. NPA charges for different structural arrangements of $M_2P_4H_4$ model complexes.[a]

Structure atom:	M	P_A	P_B	$H(P_A)$	$H(P_B)$
"$K_2P_4Mes_4$"	+0.887	−0.671	−0.139	−0.045	−0.034
"Na_2P_4Mes"	+0.847	−0.678	−0.114	−0.025	−0.016
"$Na_2P_4Ph_4$"	+0.831	−0.810	−0.018	+0.012	−0.051
"Na_2P_4tBu"	+0.825	−0.789	−0.014	+0.016	−0.037

[a] B3PW91/IGLO-III level (DZVP basis for M). Average values for almost symmetry-equivalent positions.

thus determined mainly by the structure in solution and/or the solid state. As our calculations, which are based on parameters taken from the solid-state structures, reproduce well the principal trends in $J(P_A,P_{B'})$, $J(P_B,P_{B'})$, and $J(P_A,P_{A'})$ from NMR in solution, it is very likely that the solution structures are similar to the solid-state ones. This suggests contact-ion pairs in solution, as had already been presumed.[12,13] A dihedral angle α near 0° (*syn*-periplanar arrangement, type II) gives large negative $J(P_B,P_{B'})$ (ca. −300 Hz), very small negative $J(P_A,P_{B'})$, and relatively large, positive $J(P_A,P_{A'})$ (ca. +200 to +300 Hz). Dihedral angles α near 75° (type I) provide less negative $J(P_B,P_{B'})$ (ca. −125 Hz), positive $J(P_A,P_{B'})$ near 100 Hz but very small $J(P_A,P_{A'})$. Note that we avoid designations $^2J(P_A,P_{B'})$ or $^3J(P_A,P_{A'})$, due to the fact that both of these couplings involve appreciable through-space coupling contributions (see below). The only coupling that appears to be relatively independent of structure is $^1J(P_A,P_B)$. It tends to be in the −310 Hz to −340 Hz range for all systems.

Conformational study: Given that the main structural effects on the couplings appear to be preserved in calculations for the free $P_4H_4^{2-}$ anion (Table 2), we could utilize the free anion models for further investigations of the conformational dependence of the couplings. We have carried out a scan of dihedral angle α by varying it in steps of 10° and allowing β and γ to relax. Energies for these partially relaxed scans are shown in Figure 2a. Depending on the sign of α we chose initially, we identified two conformationally different series of arrangements we will call conformer C1 and C2, respectively. Conformer C1 was obtained initially for negative α values of the RR enantiomer. However, the *S*,*S* enantiomer with positive α will have identical energies and coupling constants. When starting with positive α of the *R*,*R* isomer, we obtained a different series, called conformer C2 (no *meso* isomers were studied). We noted that there was a discontinuity in energies (Figure 2a) and coupling constants (see below) for this series near $\alpha = 20°$. When scanning β for fixed values of α between 0 and 30°, we noted a change of conformational preferences in β with increasing α (Figure 2b): While a minimum of β near −140° is preferred initially, a second minimum with β near −100° develops gradually. It is developed and is lower than the initial conformer at $\alpha = 20°$, and the first minimum vanishes at $\alpha = 30°$. We will call the initial structures with β near −140° conformer C2′ in the following (cf. Figure 2a).

Preferred values of β and γ as functions of α are shown for the different series in Figure 3a and b, respectively. We also provide the corresponding values extracted from the four experimental structures discussed above for comparison. Looking at β first (Figure 3a), we note that, at their respective α values three of the four structures exhibit β values near our conformational curves C2′ ("$Na_2P_4tBu_4$") or C1 ("$Na_2P_4Mes_4$" and "$K_2P_4Mes_4$"), whereas the β value of the "$Na_2P_4Ph_4$" structure is more negative than obtained for any of the curves. The γ values for all experimental structures are about 10° larger than found for any of the curves.

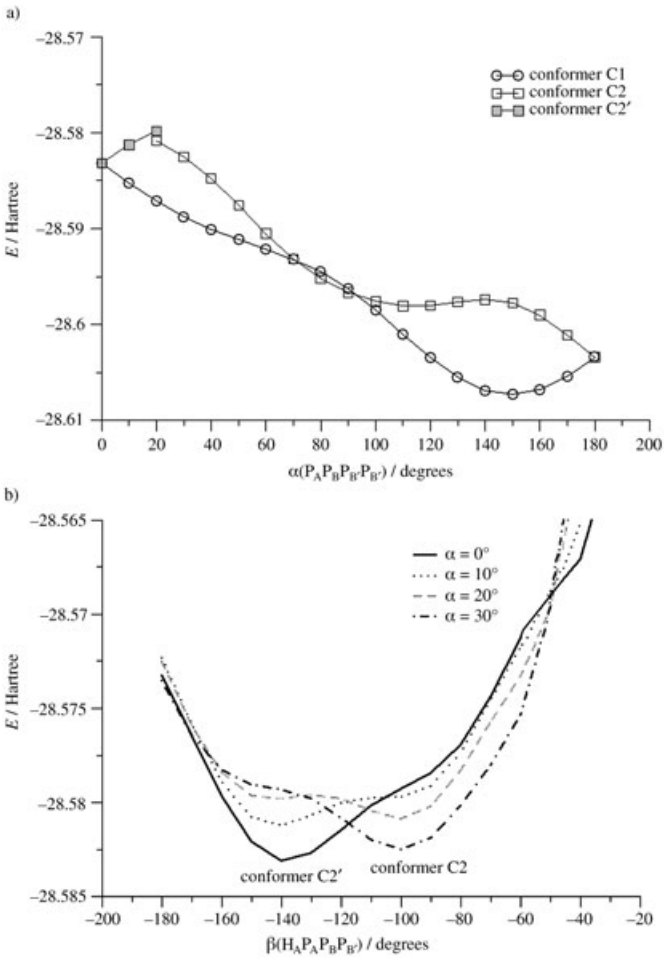

Figure 2. Conformational energy dependence of the $P_4H_4^{2-}$ anion. a) As function of dihedral angle $\alpha = d(P_A\text{-}P_B\text{-}P_{B'}\text{-}P_{A'})$. b) Additional minimum in $\beta = d(H[P_A]\text{-}P_A\text{-}P_B\text{-}P_{B'})$ for $\alpha = 20°$. Distances and angles were kept fixed during changes of dihedral angles.

These deviations of our computed conformational curves for the small $P_4H_4^{2-}$ model from experiment reflect most likely the steric influence of the organic substituents, as well as some environmental effects for the "real systems". This is of course also expected to influence the coupling constants as discussed below. On the potential energy surface of our small model anion, we expect more minima, in particular with β values below 90°. However, these arrangements are unlikely to get realized for the true systems, due to the steric requirements of the substituents.

Turning now to the "Karplus-type" curves of coupling constants as functions of α (Figure 4), we note a relatively small dependence on α for $J(P_A,P_B)$, with values mostly in the range between −180 and −280 Hz, as one might have expected for this one-bond coupling (Figure 4a; in the range below $\alpha = 40°$, curve C2 is probably not a very realistic model). Similarly, the range of $J(P_B,P_{B'})$ is restricted between −150 and −300 Hz (Figure 4b). The "experimental" conformations (cf. free anion results in Table 2) all led to appreciably more negative $J(P_A,P_B)$ (Figure 4a), probably due to the more positive γ (cf. Figure 3b). In contrast, the $J(P_B,P_{B'})$

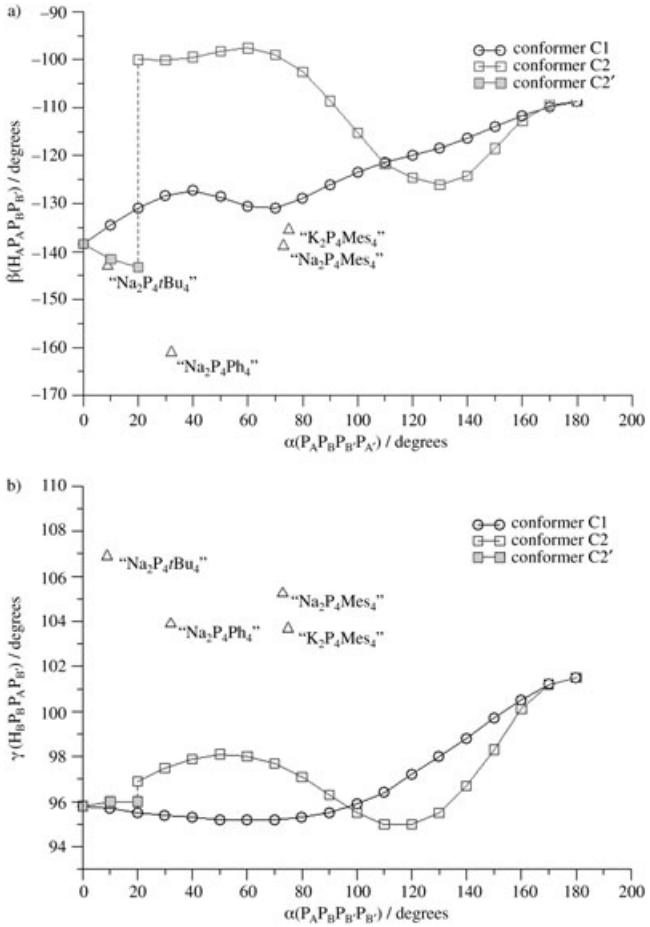

Figure 3. Interdependence of different dihedral angles. Squares and circles connected by lines represent partial optimizations of free $P_4H_4^{2-}$. For comparison, the corresponding values from the experimental structures are shown (open triangles). Conformer C1 was initially obtained for an enantiomer with negative α, conformer C2 for positive α. A second minimum in β (conformer C2′, $\beta \approx -140°$ compared to $\beta \approx -100°$ for conformer C2) develops at $\alpha = 20°$ (cf. Figure 2b). This leads to discontinuities in both curves. a) β as function of α. b) γ as function of α. Note that further conformers, that are unrealistic for substituted species, have been omitted.

values of the "experimental" conformations give couplings either somewhat too negative for type II or somewhat too positive for type I.

The $J(P_A,P_{B'})$ couplings (Figure 4c) exhibit very large conformational dependencies, not only on α, but obviously also on β. The "experimental" structures give either values close to the conformer C1 curve (type II, "$Na_2P_4tBu_4$" and "$Na_2P_4Ph_4$"; cf. the very small couplings) or much too large positive ones (type I, "$Na_2P_4Mes_4$" and "$K_2P_4Mes_4$"). It appears that for small α, these $J(P_A,P_{B'})$ couplings are generally small, without much dependence on the substituent confor-

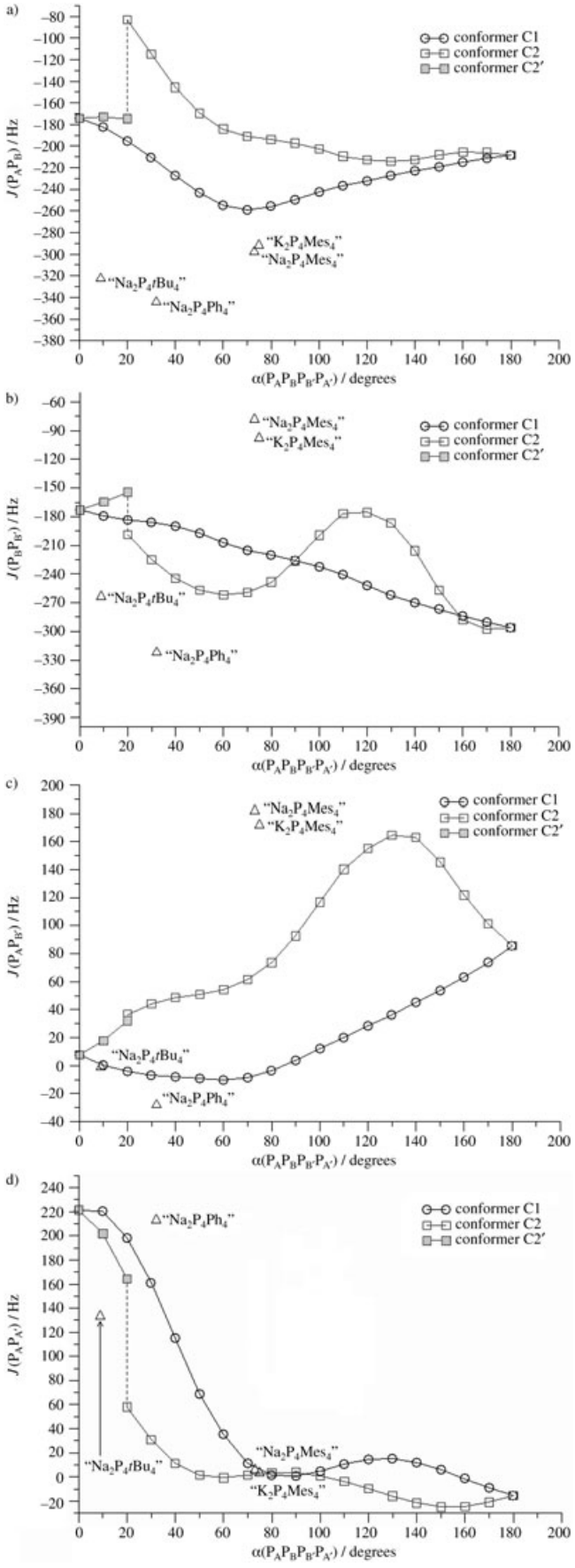

Figure 4. Computed Karplus-type relations for P–P coupling constants with respect to dihedral angle α (P_A-P_B-$P_{B'}$-$P_{A'}$). Circles and squares connected by lines represent results for partially optimized free anions $P_4H_4^{2-}$. Results at experimental dihedral angles shown for comparison as open triangles. a) $J(P_A,P_B)$. b) $J(P_B,P_{B'})$. c) $J(P_A,P_{B'})$. d) $J(P_A,P_{A'})$.

mation. For larger α values, the substituent conformation (in this case probably γ; cf. Figure 3b) plays a larger role.

Finally, the $J(P_A,P_{A'})$ couplings (Figure 4d) exhibit appreciable variation for small α values but decrease quickly to values near 0 Hz above $\alpha = 40°$ and remain relatively constant for larger α values. The results for the type I "experimental" structures ("$Na_2P_4Mes_4$" and "$K_2P_4Mes_4$") are in this range of small couplings and do not seem to be influenced much by deviations of β or γ from our conformational curves. In contrast, the coupling for the "$Na_2P_4tBu_4$" structure is too low, and that for the "$Na_2P_4Ph_4$" structure is above the curve of conformer C1 (Figure 4d).

These results indicate that the couplings are predominantly determined by the structure of the $P_4R_4^{2-}$ unit. While the dihedral angle α of the phosphorus framework is the most important parameter, the substituent conformation influences some of the couplings via the dihedral angles β and γ. In cases where α renders the couplings very small, the values of β and γ play only a minor role for the coupling constants. The different formal bond topologies of type I versus type II systems (Figure 1) are only of indirect importance. They influence the couplings mainly by tuning the conformation of the anion, together with steric interactions between the substituents. Additional electrostatic influences from the metal cations are in most cases only of secondary importance for the predominant Fermi-contact mechanism of spin–spin coupling [but note $J(P_A,P_{A'})$ in the type II structures, cf. Table 2].

ELF analyses: To rationalize the observed trends, we have carried out further analyses of real space functions. Isosurface plots of the electron localization function (ELF[30]) in Figure 5 indicate particularly the relative positions of the "free electron pairs" on the phosphorus atoms. We expected that the orientation of the two lone pairs on P_A relative to the single lone pair on $P_{B'}$ will be important for the conformational dependence of $J(P_A,P_{B'})$, due to "through-space" interactions between these free electron pairs (see refs. [1,28]). The relative orientation of the two lone pairs on P_B and $P_{B'}$ may influence possible through-space contributions to the one-bond coupling $J(P_B,P_{B'})$. Similarly, the relative orientations of the overall four lone pairs on P_A and $P_{A'}$ may determine the conformational dependence of the through-space component of $J(P_A,P_{A'})$. These expectations fit very nicely with the actual positions of the lone-pair ELF domains in Figure 5: In the "*gauche*" conformation of the "$Na_2P_4Mes_4$" structure ($\alpha = 73°$), the alignment of the P_A and $P_{A'}$ lone pairs is unfavorable for through-space interactions, whereas the P_A and $P_{B'}$ lone pairs are more or less aligned. In the almost *syn*-periplanar "$Na_2P_4Ph_4$" structure ($\alpha = 321°$), matters are opposite, with good P_A–$P_{B'}$ and poor P_A–$P_{A'}$ lone-pair alignment. This fits the experimental and computational observation of large $J(P_A,P_{B'})$ and small $J(P_A,P_{A'})$ in the "$Na_2P_4Mes_4$" structure, as well as small $J(P_A,P_{B'})$ and large $J(P_A,P_{A'})$ in the "$Na_2P_4Ph_4$" structure (Table 2). The *syn*-periplanar arrangement of the two lone pairs on P_B and $P_{B'}$ in the type II structures (Figure 5b) may lead to appreciable through-space interactions between these lone pairs for $J(P_B,P_{B'})$, whereas the two lone pairs are aligned unfavorably for the type I structures (Figure 5a). Consequently, the B,B′ couplings are considerably more negative for the former systems (Table 2).

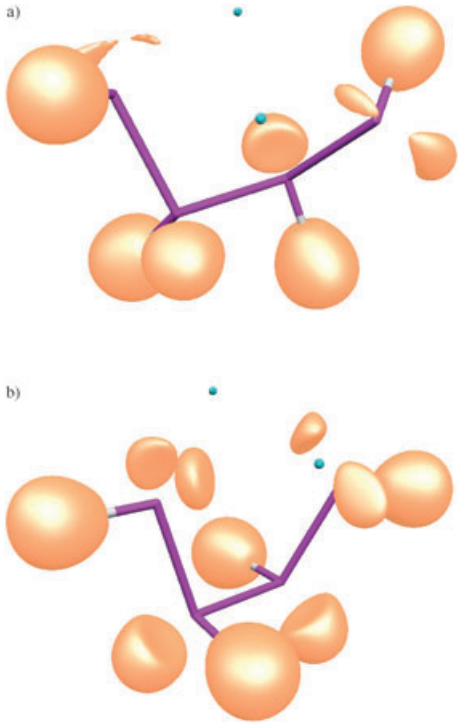

Figure 5. Isosurface plots of electron localization function (ELF = 0.9406). a) "Na_2P_4Mes". b) "$Na_2P_4Ph_4$".

Visualization of coupling pathways by CED: To further support these interpretations via through-space lone-pair contributions to the coupling constants, we have computed the coupling energy densities for these two systems. The coupling energy density (CED) introduced by Malkina and Malkin[28] is a real-space function in the sense of property densities discussed by Buckingham and Jameson[33] (see also ref. [34]). It integrates to the reduced coupling constant when taken over all of space [cf. Eq. (1)]. CED provides a powerful first-principles tool for the visualization of coupling pathways, independent of unitary transformations of the orbital basis. In particular, it has already been shown that through-space and through-bond contributions to couplings may be distinguished nicely in displays of CED.[1,28]

Consistent with the above discussion of the ELF isosurface plots, the CED isosurface plots for $J(P_A,P_{B'})$, $J(P_A,P_{A'})$, and $J(P_B,P_{B'})$ in Figure 6 confirm appreciable contributions from through-space interactions between the respective phosphorus lone pairs for $J(P_A,P_{A'})$ in the "$Na_2P_4Ph_4$" structure (Figure 6d, $\alpha = 32°$) and equally pronounced through-space contributions to $J(P_A,P_{B'})$ in the "$Na_2P_4Mes_4$" structure (Figure 6a, $\alpha = 73°$). The CED exhibits an oscillatory behavior as observed previously. The CED plots for $J(P_A,P_{A'})$ in

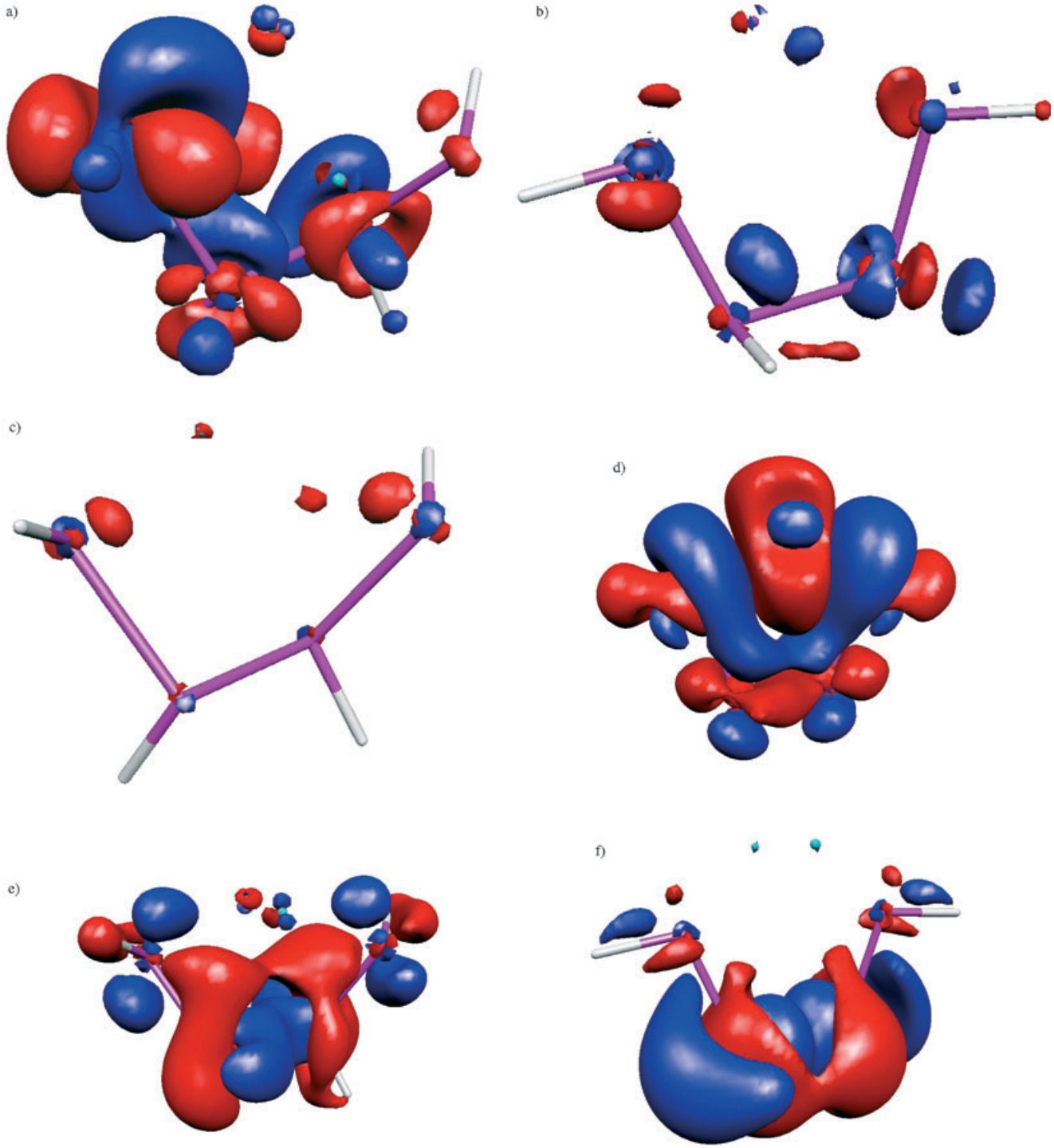

Figure 6. Isosurface plots of Coupling Energy Density (blue and red isosurfaces indicate positive and negative CED, respectively). a) "Na_2P_4Mes", $J(P_A,P_{B'})$ (isosurface = +/−1.0); b) "$Na_2P_4Ph_4$", $J(P_A,P_{B'})$ (isosurface = +/−1.0); c) "Na_2P_4Mes" $J(P_A,P_{A'})$ (isosurface = +/−0.5); d) "$Na_2P_4Ph_4$", $J(P_A,P_{A'})$ (isosurface = +/−0.5); e) "$Na_2P_4Mes_4$" $J(P_B,P_{B'})$ (isosurface = +/−1.0); f) "$Na_2P_4Ph_4$" $J(P_B,P_{B'})$ (isosurface = +/−1.0).

the syn-periplanar "$Na_2P_4Ph_4$" structure in Figure 6d resemble very much analogous plots for an organic *cis*-bisphosphine (Figure 3 in ref. [28]), where appreciable through-space contributions to J(P,P) were identified. When taking the same CED isosurface values for the corresponding "unfavorable" conformations [$J(P_A,P_{A'})$ in the "$Na_2P_4Mes_4$" structure, Figure 6c; and $J(P_A,P_{B'})$ in the "$Na_2P_4Ph_4$" structure, Figure 6b], the magnitudes of the CED peaks are obviously dramatically diminished, consistent with the small coupling constants in these cases (recall that the space integral of CED gives the reduced coupling constant). In Figure 7a, the smaller isosurface value for $J(P_A,P_{A'})$ in the *gauche* ori-

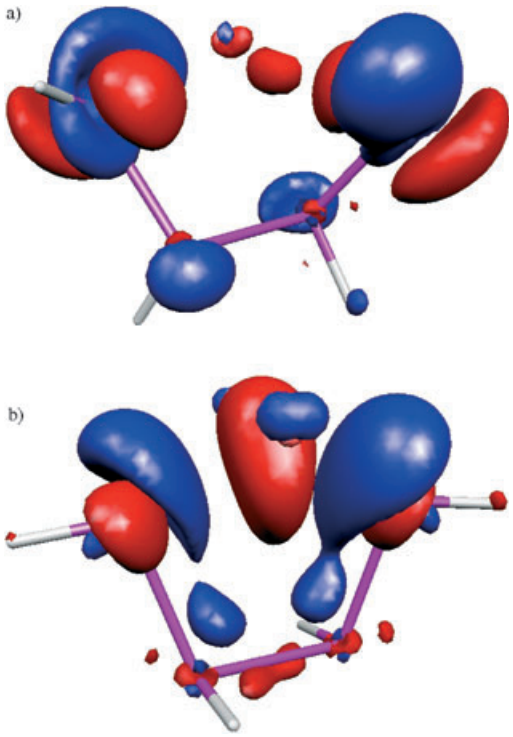

Figure 7. Further CED isosurface plots for $J(P_A,P_{A'})$ (blue and red isosurfaces indicate positive and negative CED, respectively). a) "Na_2P_4Mes" $J(P_A,P_{A'})$ (isosurface = +/−0.1); b) "$Na_2P_4Ph_4$", $J(P_A,P_{A'})$ (isosurface = +/−2.5).

entation gives a "blow-up" of the CED and allows the unfavorable through-space pathway to be observed more clearly (cf. also Figure 6c). The remaining very small coupling constant (cf. Table 2) may be viewed as a composite from small through-space and equally small through-bond contributions. Figure 7b uses a larger CED isosurface value to deconvolute the very large oscillations for the syn-periplanar case in Figure 6d. This visualization suggests that through-space coupling dominates but through-bond ^3J coupling contributes also to $J(P_A,P_{A'})$.

CED isosurfaces for $J(P_B,P_{B'})$ are shown in Figure 6e for the "$Na_2P_4Mes_4$" structure (type I) and in Figure 6f for the "$Na_2P_4Ph_4$" structure (type II). In both cases, we may clearly distinguish a positive through-bond contribution (blue isosurface) and a negative through-space contribution (red isosurface). For the syn-periplanar arrangement of the two phosphorus lone pairs in the type II arrangement (cf. Figure 5b), the negative through-space contribution is obviously enhanced considerably, leading to an overall more negative coupling constant (Figure 6f; cf. Table 2).

Through the combination of ELF and CED visualization, the structural dependence of the $J(P_A,P_{A'})$, $J(P_A,P_{B'})$ and $J(P_B,P_{B'})$ coupling constants may thus be rationalized mainly by an orientational dependence of through-space interactions between appropriate phosphorus lone pairs.

Conclusions

Spin–spin coupling constants obtained from NMR experiments can provide deep insights into molecular and electronic structure, but their detailed interpretation may be difficult without support from quantum chemical calculations.[1] In the present work, we have chosen the very interesting experimental coupling constants for four structurally characterized alkali metal tetraphosphane-1,4-diides as a basis for detailed analyses by state-of-the-art quantum chemical methods. Our main conclusions may be summarized as follows:

a) The experimentally characterized structures of the contact ion pairs between alkali metal cations and $P_4R_4^{2-}$ anions are apparently preserved in solution. This is supported by the good agreement of computed J(P,P) couplings based on experimental solid-state structures and the solution NMR data.
b) The influence of the metal cations on the J(P,P) couplings is mainly due to a structural role, as the conformation within the anion depends partly on interactions with the cation. Additional electrostatic effects of the cations on the couplings are notable but of secondary importance. Contributions to the couplings through covalent P–M bonding have not been identified. This is an important result that will bear also on many other contact ion pair arrangements. Similar arguments pertain to the interrelations between spin–spin coupling across hydrogen bonds and the covalency of these hydrogen bonds.[5,6]
c) The significant, characteristic conformational dependence of $J(P_B,P_{B'})$, $J(P_A,P_{B'})$, and $J(P_A,P_{A'})$ is due to through-space coupling, which depends on the relative orientation of appropriate free electron pairs on phosphorus. This has been shown graphically, by using a combination of real-space functions, the coupling energy density (CED) and the electron localization function (ELF). In the area of oligophosphanes and oligophosphanides, this is to our knowledge the first clear verification of the frequent implicit assumption[9,10] that the free electron pairs on phosphorus are involved in the spin–spin couplings.

We expect that similar analyses will help to shed light also on coupling pathways and conformational dependences of spin–spin couplings in many other cases.

Acknowledgements

We thank R. Wolf and E. Hey-Hawkins (Leipzig) for suggesting the study of the title systems, for illuminating discussions, and for providing experimental structure data, as well as a copy of ref. [12] prior to publication. We are also grateful to M. Westerhausen (Jena) and to V. G. Malkin (Bratislava) for helpful discussions. This work has been supported by Deutsche Forschungsgemeinschaft (project KA1187/5–1). Work in Bratislava has been supported by the Slovak Grant Agencies VEGA (No. 2/3103/23) and APVT (No. 51-045502), as well as COST D18 action.

[1] See, for example: O. L. Malkina *Interpretation of Nuclear Spin–spin Coupling Constants,* in *Calculation of NMR and EPR Parameters. Theory and Applications* (Eds.: M. Kaupp, M. Bühl, V. G. Malkin), Wiley-VCH, Weinheim, **2004**, Chapter 19, pp. 305–322.
[2] See, for example: R. K. Harris, *Nuclear Magnetic Resonance Spectroscopy*, Pitman, London, **1983**.
[3] See, for example: W. D. Arnold, J. Mao, H. Sun, E. Oldfield, *J. Am. Chem. Soc.* **2000**, *122*, 12164, and references therein.
[4] See, for example: J. E. Del Bene *Characterizing Two-Bond ^{13}C–^{15}N, ^{15}N–^{15}N, and ^{19}F–^{15}N Spin–spin Coupling Constants across Hydrogen Bonds in ab inito EON-CCSD Calculations,* in *Calculation of NMR and EPR Parameters. Theory and Applications* (Eds.: M. Kaupp, M. Bühl, V. G. Malkin), Wiley-VCH, Weinheim, **2004**, Chapter 22, pp. 353–370.
[5] See, for example: J. E. Del Bene, *J. Phys. Chem. A* **2004**, *108*, 6820, and references therein.
[6] D. L. Bryce, R. E. Wasylishen, *J. Mol. Struct.* **2002**, *602*/603, 463; W. D. Arnold, E. Oldfield, *J. Am. Chem. Soc.* **2000**, *122*, 12835.
[7] V. M. S. Gil, W. von Philipsborn, *Magn. Reson. Chem.* **1989**, *27*, 409–430; J. G. Verkade, *Coord. Chem. Rev.* **1972**/**1973**, *9*, 1; P. S. Pregosin, R. W. Kunz, *^{31}P and ^{13}C NMR of Transition Metal Phosphine Complexes*, Springer, Berlin, **1979**.
[8] For experimental examples of appreciable ^{2}J(P,P) couplings in phosphanides across alkaline earth cations, compare: M. Westerhausen, M. H. Digeser, M. Krofta, N. Wiberg, H. Nöth, J. Knizek, W. Ponikwar, T. Seiferth, *Eur. J. Inorg. Chem.* **1999**, 743; M. Westerhausen, C. Birg, M. Krofta, P. Mayer, T. Seifert, H. Nöth, A. Pfitzner, H.-J. Deiseroth, *Z. Anorg. Allg. Chem.* **2000**, *626*, 1073; M. Westerhausen, M. Krofta, *Z. Anorg. Allg. Chem.* **2000**, *626*, 2307.
[9] See, for example: M. Baudler, G. Reuschenbach, J. Hellmann, J. Hahn, *Z. Anorg. Allg. Chem.* **1983**, *499*, 89; M. Baudler, G. Reuschenbach, J. Hahn, *Chem. Ber.* **1983**, *116*, 847.
[10] See, for example: I. Kovacs, H. Krautscheid, E. Matern, E. Sattler, G. Fritz, W. Hönle, H. Borrmann, H. G. von Schnering, *Z. Anorg. Allg. Chem.* **1996**, *622*, 1564.
[11] N. Wiberg, A. Wörner, K. Karaghiosoff, D. Fenske, *Chem. Ber. Recueil* **1997**, *130*, 135.
[12] R. Wolf, A. Schisler, P. Lönnecke, C. Jones, E. Hey-Hawkins, *Eur. J. Inorg. Chem.* **2004**, 3277.
[13] M. Baudler, D. Koch, *Z. Anorg. Allg. Chem.* **1976**, *425*, 227.
[14] J. Geyer, J. Harmer, H. Grützmacher, *Angew. Chem.* **2004**, *116*, 4185; *Angew. Chem. Int. Ed.* **2004**, *43*, 4093; see also: J. Geyer, H. Rüegger, M. Wörle, H. Grützmacher, *Angew. Chem.* **2003**, *115*, 4081; *Angew. Chem. Int. Ed. Engl.* **2003**, *42*, 3951.
[15] See, for example: H. Benedict, I. G. Shenderovich, O. L. Malkina, V. G. Malkin, G. S. Denisov, N. S. Golubev, H.-H. Limbach, *J. Am. Chem. Soc.* **2000**, *122*, 1979.
[16] Gaussian 03, Revision A1, M. J. Frisch, G. W. Trucks, H. B. Schlegel, G. E. Scuseria, M. A. Robb, J. R. Cheeseman, J. A. Montgomery, J. T. Vreven, K. N. Kudin, J. C. Burant, J. M. Millam, S. S. Iyengar, J. Tomasi, V. Barone, B. Mennucci, M. Cossi, G. Scalmani, N. Rega, G. A. Petersson, H. Nakatsuji, M. Hada, M. Ehara, K. Toyota, R. Fukuda, J. Hasegawa, M. Ishida, T. Nakajima, Y. Honda, O. Kitao, H. Nakai, M. Klene, X. Li, J. E. Knox, H. P. Hratchian, J. B. Cross, C. Adamo, J. Jaramillo, R. Gomperts, R. E. Stratmann, O. Yazyev, A. J. Austin, R. Cammi, C. Pomelli, J. W. Ochterski, P. Y. Ayala, K. Morokuma, G. A. Voth, P. Salvador, J. J. Dannenberg, V. G. Zakrzewski, S. Dapprich, A. D. Daniels, M. C. Strain, O. Farkas, D. K. Malick, A. D. Rabuck, K. Raghavachari, J. B. Foresman, J. V. Ortiz, Q. Cui, A. G. Baboul, S. Clifford, J. Cioslowski, B. B. Stefanov, G. Liu, A. Liashenko, P. Piskorz, I. Komaromi, R. L. Martin, D. J. Fox, T. Keith, M. A. Al-Laham, C. Y. Peng, A. Nanayakkara, M. Challacombe, P. M. W. Gill, B. Johnson, W. Chen, M. W. Wong, C. Gonzalez, J. A. Pople, Pittsburgh PA, **2003**.
[17] A. D. Becke, *J. Chem. Phys.* **1993**, *98*, 5648.
[18] J. P. Perdew, Y. Wang, *Phys. Rev. B* **1992**, *45*, 13244; J. P. Perdew in: *Electronic Structure of Solids* (Eds.: P. Ziesche, H. Eischrig), Akademie Verlag, Berlin, **1991**; J. P. Perdew, J. A. Chevary, S. H. Vosko, K. A. Jackson, M. R. Pederson, D. J. Singh, C. Fiolhais, *Phys. Rev. B* **1992**, *46*, 6671.
[19] A. Bergner, M. Dolg, W. Kuechle, H. Stoll, H. Preuss, *Mol. Phys.* **1993**, *80*, 1431.
[20] T. H. Dunning, *J. Chem. Phys.* **1970**, *53*, 2823.
[21] V. G. Malkin, O. L. Malkina, R. Reviakine, A. V. Arbuznikov, M. Kaupp, B. Schimmelpfennig, I. Malkin, T. Helgaker, K. Ruud, ReSpect program, version 1.1, **2002**.
[22] V. G. Malkin, O. L. Malkina, L. A. Eriksson, D. R. Salahub, in Modern *Density Functional Theory: A Tool for Chemistry; Theoretical and Computational Chemistry*, *Vol. 2* (Eds.: J. M. Seminario, P. Politzer), Elsevier, Amsterdam, **1995**; O. L. Malkina, D. R. Salahub, V. G. Malkin, *J. Chem. Phys.* **1996**, *105*, 8793.
[23] A. D. Becke, *Phys. Rev. A* **1988**, *38*, 3098.
[24] J. P. Perdew, *Phys. Rev. B* **1986**, *33*, 8822.
[25] J. P. Perdew, Y. Wang, *Phys. Rev. B* **1986**, *33*, 8800.
[26] N. Godbout, D. R. Salahub, J. Andzelm, E. Wimmer, *Can. J. Chem.* **1992**, *70*, 560.
[27] W. Kutzelnigg, U. Fleischer, M. Schindler, in *NMR-Basic Principles and Progress*, *Vol. 23*, Springer, Heidelberg, **1990**, pp. 165–262; S. Huzinaga *Approximate Atomic Functions*, University of Alberta, **1971**.
[28] O. L. Malkina, V. G. Malkin, *Angew. Chem.* **2003**, *115*, 4471; *Angew. Chem. Int. Ed.* **2003**, *42*, 4335.
[29] MOLEKEL 4.0, P. Flükiger, H. P. Lüthi, S. Portmann, J. Weber, Swiss Center for Scientific Computing, Manno (Switzerland), **2000**; see, for example: S. Portmann, H. P. Lüthi, *Chimia* **2000**, *54*, 766.
[30] A. D. Becke, K. E. Edgecombe, *J. Chem. Phys.* **1990**, *92*, 5397; A. Savin, A. D. Becke, J. Flad, R. Nesper, H. G. von Schnering, *Angew. Chem.* **1991**, *101*, 421; *Angew. Chem. Int. Ed. Engl.* **1991**, *30*, 409.
[31] S. Noury, X. Krokidis, F. Fuster, B. Silvi, TopMoD package, Université Pierre et Marie Curie, **1997**.
[32] A. E. Reed, F. Weinhold, *J. Chem. Phys.* **1985**, *83*, 1736.
[33] C. J. Jameson, A. D. Buckingham, *J. Chem. Phys.* **1980**, *73*, 5684; C. J. Jameson, A. D. Buckingham, *J. Phys. Chem.* **1979**, *83*, 3366.
[34] A. Soncini, P. Lazzeretti, *J. Chem. Phys.* **2003**, *118*, 7165.

Received: November 3, 2004
Published online: March 2, 2005